PERGAMON

International Journal of Heat and Mass Transfer 46 (2003) 497–512

International Journal of HEAT and MASS TRANSFER

www.elsevier.com/locate/ijhmt

Chimney-enhanced natural convection from a vertical plate: experiments and numerical simulations

S. Kazansky, V. Dubovsky, G. Ziskind *, R. Letan

Department of Mechanical Engineering, Heat Transfer Laboratory, Ben-Gurion University of the Negev, P.O. Box 653, Beer-Sheva, Israel

Received 14 May 2001; received in revised form 24 June 2002

Abstract

This study deals with natural-convection heat transfer from a vertical electrically heated plate, which is symmetrically placed in a chimney of variable height. The heated plate serves as a thermal pump for ventilation of a symmetrical enclosure beneath the chimney.

In order to provide a comprehensive picture of the phenomena, three main approaches are used in parallel: temperature and velocity measurements, flow visualization, and numerical simulation. Temperature measurements are done by thermocouples distributed inside the plate and through the chimney. Velocity measurements are performed by means of a precise anemometer. Visualization is performed using smoke of incense sticks, with video recording and consequent image processing. Computer simulations of unsteady flow and temperature fields are performed in 3D and compared with measurements and visualization, with special attention paid to velocity fluctuations. Analysis is presented on the dependence of the temperature distribution on the flow field. The air flow rate on the heating plate in the chimney increases with the chimney height and is adequately predicted by the numerical simulation of the system.

Keywords: Natural convection; Chimney effect; Vertical plate; Temperature and flow field; Visualization

1. Introduction

The present work is an additional step in an extensive study being performed in our laboratory on different aspects of passive ventilation of structures. In the previous laboratory-scale study [1], ventilation of an enclosure by air flow induced from a heated downward-facing plate has been studied both experimentally and numerically. Numerical studies have been performed also for one- and multi-story real-size structures, while extensive experimental investigations were done for their laboratory-scale models [2–4].

The problem addressed in the present work is, essentially, chimney-enhanced free convection from a heated vertical plate. Chimney effect was studied in the past, however, as noted recently by Fisher and Torrance [5], "very few prior experiments have considered chimney-enhanced convection." Following their own theoretical analysis [6,7], Fisher and Torrance [5] report experimental results of chimney enhanced heat transfer from a vertical parallel-plate heat sink. They conclude that chimneys can provide significant heat transfer enhancement.

Sparrow et al. [8] analyzed numerically the heat transfer rate from a single isothermal vertical plate and that for a plate that is shrouded by an adiabatic wall situated parallel to the plate. Haaland and Sparrow [9] obtained numerical solutions for a parallel-walled chimney, where the flow is induced by heat sources located in its inlet. Straatman et al. [10] performed a numerical and experimental study of free convection in an isothermal parallel-walled channel, to which adiabatic extensions of various sizes and shapes were added. Later

* Corresponding author. Tel.: +972-8-647-7089; fax: +972-8-647-2813.

E-mail address: gziskind@bgumail.bgu.ac.il (G. Ziskind).

0017-9310/03/$ - see front matter
PII: S0017-9310(02)00268-5

Nomenclature

g	gravitational acceleration (m/s^2)
h	static enthalpy (J/kg)
H	unit height (= 150 mm)
I	radiation intensity (W/m^2)
k	thermal conductivity (W/m K)
L	length (m)
p	pressure (Pa)
p'	modified pressure (Pa)
Ra	Rayleigh number ($= g\beta[T_p - T_\infty]L^3/v\alpha$)
Re	Reynolds number ($= u\Delta/v$)
t	time (s)
T	temperature (K or °C)
u	velocity (m/s)
x	distance (m)

Greek symbols

α	thermal diffusivity (m^2/s)
β	thermal expansion coefficient (K^{-1})
Δ	plate thickness (m)
ε	emissivity
μ	dynamic viscosity (kg/m s)
v	kinematic viscosity (m^2/s)
ρ	density (kg/m^3)
τ	stress tensor (N/m^2)
Ω	solid angle

Subscripts

i, j	component
p	plate
r	radiation
w	wall
∞	ambient

on, Shanin and Floryan [11] studied the increase of the heat transfer in systems of channels with adiabatic extensions.

Experimental results reported in the literature concern chimneys of relatively small size, suitable for cooling of electronic components. This study has been performed on a chimney of a horizontal cross-section which is approaching those of the channels examined for ventilation in real-sized buildings [2–4]. A comprehensive picture of the problem is presented, including both the resulting heat transfer enhancement and subtle details of the processes leading to it. The numerical simulations are based on the experimental parameters. That makes it possible to cross-examine the accuracy of the experiments and the validity of the simulations. Of special interest are the unsteady effects in the flow, of which the study and even detection represent a significant challenge.

In the following sections, the experimental set-up and procedure are described in detail. The numerical method is discussed, with special attention paid to its reliability in the prediction of the complex flow phenomena encountered in the present study. The results concerning the validation of the method are presented in Appendix A.

The experimental mapping of the temperature distribution inside the chimney is discussed and compared with the numerical predictions. It is shown that this distribution is related to the unsteady velocity field, characteristic of the flow inside the chimney. This flow field is revealed by smoke visualization, which is supported by the measurements and shows good agreement with the results of numerical simulations. Of particular interest is the thermal pumping effect of the heated plate in the chimney. This effect is evaluated by the mass flow rate of air through the chimney and the flow rate variation with the height of the chimney.

2. Experimental study

The experimental facility, shown in Fig. 1 and described in detail below, included an electrically heated two-sided vertical plate, an insulated chimney of variable height, an enclosure through which the air enters into the chimney, power supply to the plate, a set of thermocouples for temperature measurement inside the chimney, data acquisition system, and a smoke generation unit connected to the chimney and the enclosure. A precise anemometer has been used for velocity measurements. Smoke visualization was recorded by a digital video system. An infrared radiometer was used for estimation of the emissivities of the involved surfaces.

The heated plate was made of two identical 1.5 mm thick aluminum sheets, 150 (height) × 120 (width) mm, between which an electrical wire heater was mounted. Thus, total thickness of the plate was 5 mm. The electric power was delivered to the heater from a power supply. The maximum power input to the plate during the experiments was 40.5 W. The temperature of the plate was monitored during the experiments, using two thermocouples mounted inside the plate on both sides of the heater, to make sure that the plate is heated symmetrically. These thermocouples are denoted as TC_p in Fig. 1.

The chimney was made of two layers of cardboard, with a 20 mm layer of thermal insulation between them.

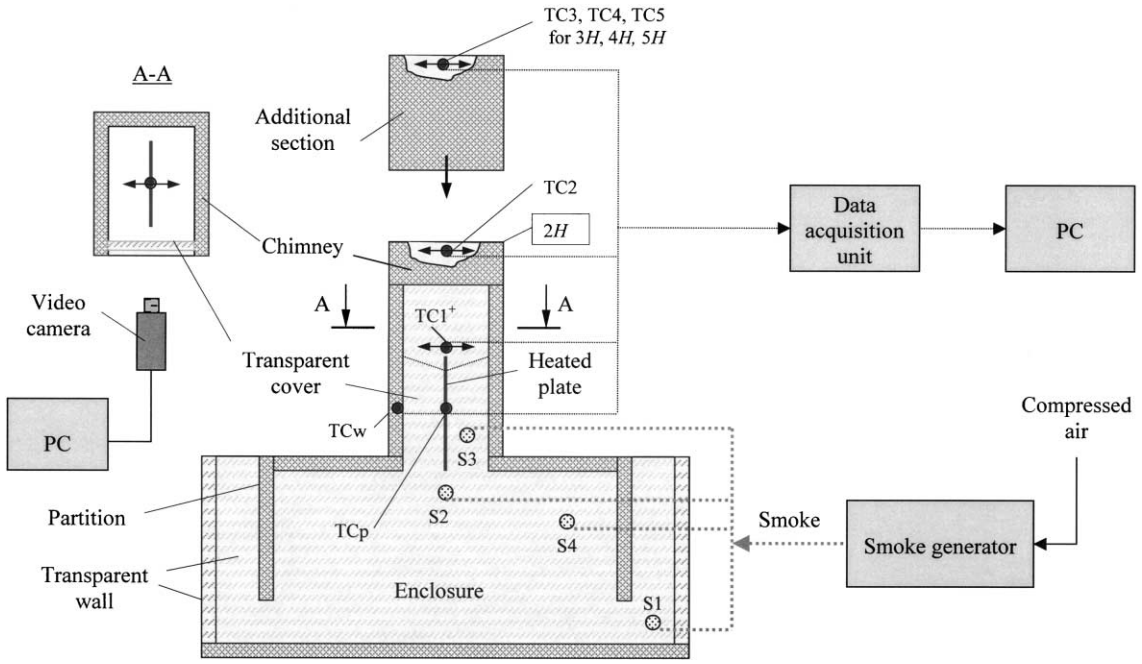

Fig. 1. General view of the experimental set-up.

The inner horizontal cross-section of the chimney is a rectangle, 180×100 mm, where the larger dimension is along the plate and the smaller one is normal to it. The bottom of the plate coincides with the bottom of the chimney. The basic height of the chimney is $2H$, where $H = 150$ mm is the vertical dimension of the heated plate.

The front bottom part of the chimney, from zero height to approximately $5/3H$, has been made of glass in order to enable observation and recording during visualization.

The chimney is modular, i.e. it is built of a number of sections. Each additional section has the height equal to the height $H = 150$ mm. The experiments were performed for the chimney of $2H$, $3H$, $4H$, $5H$, and $9H$ in height.

The enclosure from which air entered the chimney, shown in Fig. 1, is a box, of which overall inner length, height and width are 600, 300 and 240 mm, respectively. Two different boxes were used: gypsum made for measurements in the enclosure [12] and glass made for visualization. The box cover, which serves to hold the chimney, is made of pressed wood. The enclosure has partitions at its inlet ports designed to provide a well-arranged air flow inside it, as shown in the previous studies [1,12]. The distance between the partition and the sidewall of the box is 50 mm, the height of the inlet between the partition and the floor is 50 mm, and the upper entrance opening is also 50 mm wide. The flow of smoke during the visualization was observed and recorded through the transparent walls of the box.

A number of thermocouples have been used to measure the temperature of the flowing air during the experiments. As shown in Fig. 1, a thermocouple was mounted closely above the plate, i.e. at a location slightly higher than H above the entrance to the chimney. This thermocouple is denoted $TC1^+$ in the figure. A thermocouple mounted at the top of the basic $2H$ chimney is denoted TC2. Each additional section has a thermocouple at its top. According to the overall chimney height reached by the section, i.e. $3H$, $4H$, and $5H$, these thermocouples are denoted TC3, TC4, and TC5, respectively. Thus, the vertical spacing of thermocouples inside the chimney equals the height of the plate.

The thermocouples were mounted in such a way that they could be shifted across the chimney, in the direction normal to the plane of the plate itself. Thus, temperature measurements at various points were performed, and temperature profiles at various heights inside the chimney could be determined. Up to five thermocouples have been used simultaneously for the temperature measurement at different heights. Additional thermocouples monitored the temperature of the heated plate (TC_p), the temperature of the chimney wall opposite to the plate (TC_w), and the ambient temperature outside the chimney. All thermocouples were connected to a PC through a Fluke Hydra data acquisition unit.

The readings of the thermocouples were verified before each experimental run, exposing them simultaneously to the ambient air, while being connected to the data acquisitor. The time of exposure was 10–15 min. It was found that the maximum difference between the readings of any two thermocouples did not exceed 0.2 °C.

A Flir ThermaCAM SC2000 infrared radiometer has been used to estimate the emissivities, to be used in the numerical simulations. Direct infrared measurements in course of the experiments inside the chimney were not feasible. For this reason, the objects were placed vertically outside the experimental set-up, and heated up to the same typical temperature at which they are operated during the experiments. As the temperature was measured simultaneously by a thermocouple, the emissivity was adjusted until the readings of the radiometer and the thermocouple equaled. It was found that the emissivity of the cardboard was $\varepsilon_w = 0.85$. As for the plate, it was not possible to establish an accurate value of its emissivity because the plate surface had some specularity. It was also found that oxidation of the plate occurred in course of the experiments. For these reasons, the plate emissivity value was taken from the previous studies [3,4] to be equal 0.14. It should be noted that the plate emissivity does not affect the air flow rate through the chimney, as discussed later.

A typical experiment has been performed in the following manner. The chimney was mounted, and the plate was connected to the power supply and heated. The system was operated for about 2 h, until a ''stationary'' state characterized by temperature fluctuations about a certain value has been reached. Then, the readings of each thermocouple were recorded for about 10 min at each point along a horizontal line normal to the plane of the heated plate, i.e. in both the negative and positive x-direction. These readings provided the average temperature at each point, yielding further the temperature profiles shown in Fig. 2a–c for the heat input of 40.5 W. Simultaneously, temperature fluctuations have been also stored.

At the same time, the velocity of air inside the chimney has been measured by a precise, NIST traceable, TSI VelociCalc 8346 hot-wire anemometer, which has a resolution of 1.0 cm/s, an accuracy at low velocities of 1.5 cm/s, and a response time of 200 ms. The model used has an articulating probe. Both mean and fluctuating velocities were determined. The procedure was similar to that used for temperature measurements, i.e. the probe could be shifted across the chimney, yielding mean velocity profiles and velocity fluctuations, examples of which are shown in Fig. 4b–c.

When the measurements for a chimney of certain height were accomplished, an additional section of the chimney was added. It was mounted gently, while the heating of the plate was continued. As a result, the system reached, usually in about 1.5 h, a new ''stationary'' state, characterized by temperature fluctuations about another value at each point, which corresponded to the new height of the chimney. Then, all the temperature measurements were performed, both for all the points measured previously and for those of the added section.

A typical experimental run included heating of the system with the chimney of $2H$ to a ''stationary'' state, and gradual addition of the chimney sections up to heights of $3H$, $4H$, $5H$ and $9H$. Measurements were conducted at all stages. Thus, such run took usually about 12–14 h. We note here that the gradual addition of sections was important to assess the changes occurring in the system immediately.

Smoke visualization was performed both in the chimney and the glass enclosure. Incense sticks were used for smoke generation. The smoke could not be used directly, as it had to be cooled down to the ambient temperature before entering the system. For this reason, a simple but reliable ''smoke generator'' was constructed. It consisted of a transparent cylinder, 200 mm in diameter and 1 m long. The cylinder was tightly closed on both sides. One side had a small aperture, through which a long flexible transparent tube, 6 mm in diameter, connected the cylinder with the experimental set-up. Through an aperture on the other side, another small-diameter tube carried fresh air from a compressed air system. The compressed air was dispersed inside the cylinder through a ceramic dispenser. A number, typically about 15–20, of commercially available incense sticks, were placed, while smoldering, inside the transparent cylinder. Thus, after a certain amount of smoke was generated inside the cylinder, a small amount of fresh air was allowed to flow into the tube, where it provided both the oxygen needed for burning and an excessive pressure inside the cylinder, as compared to that in the experimental system. As a result, a gentle flow of smoke to the experimental set-up was established.

The smoke could not be followed all the way from the entrance of the enclosure to the exit of the chimney, as it dispersed. In order to obtain local flow patterns, the smoke has been introduced into the system at various locations, which are indicated in Fig. 1 as S1–S4. Point S1 served to release smoke at the entrance to the enclosure and to follow the flow field inside it. Point S2, located symmetrically beneath the heated plate, and point S3, located between the plate and the wall, introduced the flow of smoke directly into the chimney. Finally, point S4 has been used to record the vortex at the upper corners of the enclosure. In addition, experiments were performed with the whole box filled with smoke.

The flow of the smoke both inside the chimney and through the box has been recorded by a Redlake MotionScope 8000C digital imaging system, using a 150 W fiber optic illuminator. Examples of the recordings are shown in Figs. 5–7.

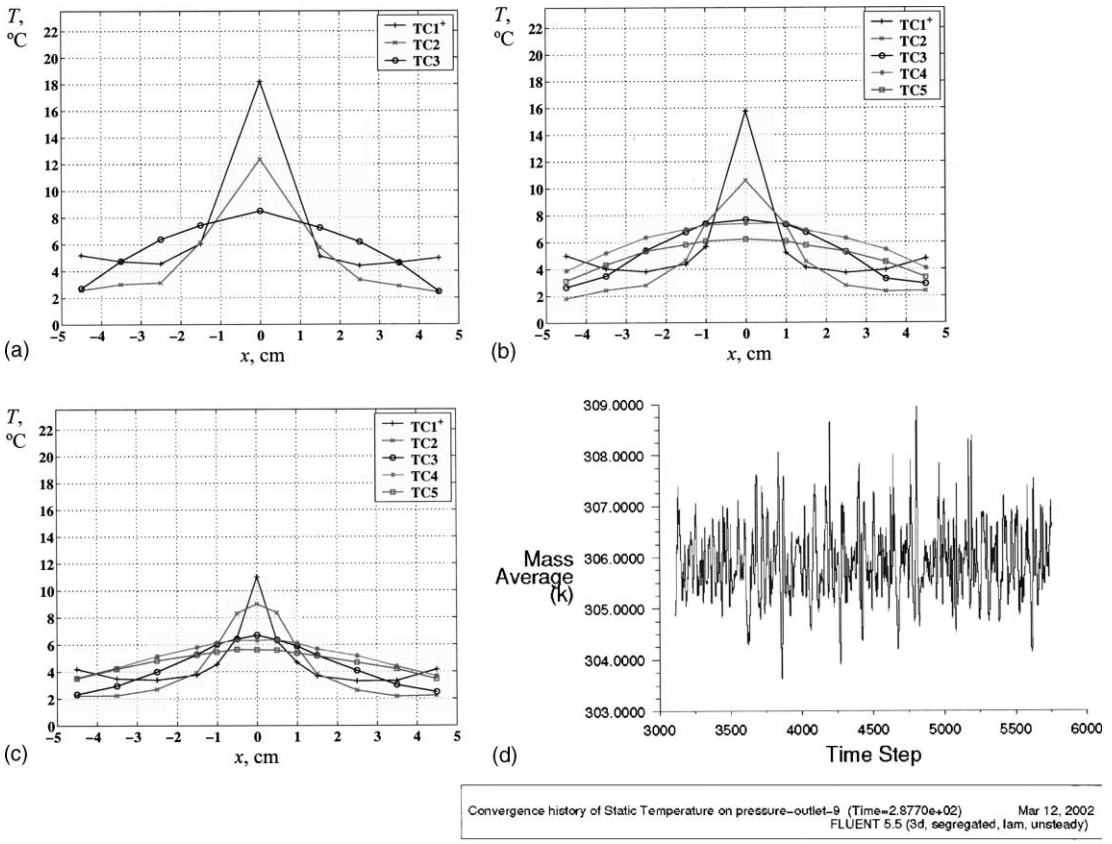

Fig. 2. Air temperatures measured across the chimney for a 40.5 W output from the plate, for different chimney heights: (a) $3H$, (b) $5H$, (c) $9H$ and (d) simulated mass-averaged temperature of the air leaving a $9H$-high chimney (300 K is taken as the ambient temperature in all numerical simulations).

The results of both the measurements and the smoke visualization indicate that the flow field is characterized by strong pulsations. In addition, in spite of the full geometrical symmetry of the system, asymmetrical flow was observed. These results are discussed later in connection with the numerical results.

3. Physical model and numerical study

The numerical calculations were performed for the velocity and temperature fields inside the chimney and the box.

The conservation equations were solved numerically, using the FLUENT 5.5 CFD software. The basic form of these equations is as follows [13]:

continuity

$$\frac{\partial \rho}{\partial t}+\frac{\partial}{\partial x_i}(\rho u_i)=0, \tag{1}$$

momentum

$$\frac{\partial}{\partial t}(\rho u_i)+\frac{\partial}{\partial x_j}(\rho u_i u_j)=-\frac{\partial p}{\partial x_i}+\frac{\partial \tau_{ij}}{\partial x_j}+\rho g_i, \tag{2}$$

energy

$$\frac{\partial}{\partial t}(\rho h)+\frac{\partial}{\partial x_i}(\rho u_i h)=\frac{\partial}{\partial x_i}\left(k\frac{\partial T}{\partial x_i}\right)+\frac{\partial p}{\partial t}+u_i\frac{\partial p}{\partial x_i}+\tau_{ij}\frac{\partial u_i}{\partial x_j} \tag{3}$$

where ρ is the density, u_i is the velocity component in the i-direction, p is the static pressure, x_i is a Cartesian coordinate, τ_{ij} is the stress tensor, g_i is the gravitational acceleration the i-direction, h is the static enthalpy, k is the thermal conductivity, T is the temperature, and t is time. Since neither large viscous stresses nor compressibility effects were expected in the current problem, the viscous heating term $\tau_{ij}(\partial u_i/\partial x_j)$ was not activated [13].

Since the flow is buoyancy driven, the momentum equation, Eq. (2), is redefined in FLUENT using the following relation for the vertical x_2-direction [13]:

$$p'=-\rho_0 g x_2+p$$

where ρ_0 is the reference density taken at 300 K and atmospheric pressure. The Boussinesq approximation was not used, and the density–temperature relation was provided as an input.

The boundary conditions for the momentum equation are no-penetration, no-slip at all the solid boundaries. The pressure boundary condition $p' = 0$ is imposed at the ports of the system, namely, at the entrance openings of the box and at the exit opening of the chimney.

The boundary conditions for the energy equation are based on the experimental parameters. The heat flux, corresponding to the input power of, for instance, 40.5 W, has been imposed on the plate. For a constant heat flux, wall temperature of the plate is not uniform. Therefore, the plate was defined in the simulations exactly as it was built in reality: it had the core which generates heat, and the external layers defined as "conducting walls." The thermal conductivity of aluminum was taken as 180 W/m K.

For the other boundaries, FLUENT makes it possible to incorporate the heat transfer coefficients of the walls and the outside temperatures in the calculation of the inside temperature field. Thus, the calculations were performed both for adiabatic walls and for walls with heat-transfer coefficients determined experimentally.

The temperature of the surroundings is imposed at the entrance opening. As for the exit opening, FLUENT adjusts the boundary condition there, extrapolating the temperature values from the interior grid cells adjacent to the exit.

Surface-to-surface radiation is taken into account through a so-called discrete transfer radiation model (DTRM). The main assumption of the DTRM is that the radiation leaving the surface element in a certain range of solid angles can be approximated by a single ray. The DTRM also assumes that all surfaces are diffuse, i.e. the reflection of incident radiation at the surface is isotropic with respect to solid angle.

At the boundaries, the DRTM is used as follows. The radiation intensity, I^-, approaching the surface is integrated to yield the incident radiation heat flux, q''^-_r, as

$$q''^-_r = \int I^- \, d\Omega \tag{4}$$

where Ω is the hemispherical solid angle. The net radiation heat flux from the surface is then computed as a sum of the reflected portion of q''^-_r and the emissive power of the surface:

$$q''^+_r = (1 - \varepsilon_w) q''^-_r + \varepsilon_w \sigma T_w^4 \tag{5}$$

where T_w is the surface temperature in Kelvin, ε_w is the wall emissivity which should be assigned as boundary condition, and $\sigma = 5.669 \times 10^{-8}$ W/m^2 K^4 is the Stefan–Boltzmann constant. FLUENT incorporates the radiation heat flux, Eq. (5), in the prediction of the wall surface temperature.

It should be noted here that the radiation model used in this study involves angular discretization in two directions. It has been found that the default values of angular divisions, equal to 2 in FLUENT, yielded some errors in the results. Therefore, the number of divisions was adjusted, and at four divisions in each direction the errors practically disappeared. This has been achieved on account of the computing time, where a typical numerical run for a $5H$-high chimney took about 30 h.

The software enables the calculation of the overall rate of change of the internal energy of the fluid, flowing from the entrance to the exit, as well as the calculation of the overall heat input at any boundary. Therefore, the comparison of these two results served to ensure the overall energy balance of the system.

The grid used in the simulations was not uniform. It was important to provide a finer grid near the boundaries, especially at the hot plate, where the flow has a boundary-layer character. Thus, the grid of variable step has been used.

In the vertical y-direction, the plate is divided into 60 cells, varying in size from 1.3 mm at the lower edge to 3.7 mm at the middle and to 0.86 mm at the top. In the horizontal z-direction, the plate has 30 cells, varying from 6.4 mm at the symmetry plane to 1.5 mm at the edges.

Due to the symmetry, numerical solutions were performed for a half of the system which preserved all the features of the full system, including two entrance ports. Total grid size was as large as 56,700 ($\times 2$ for the full system) inner elements for the enclosure, $39,600 \times 2$ inner elements for the first 150 mm of the chimney ($1H$), and $108,900 \times 2$ elements for the $9H$ high chimney. As mentioned above, the grid is finer near the heated plate, all ports, partitions, and walls of the system. Each additional section of the chimney has also a grid of variable density, where smaller cells are used near its centerline, walls, and edges. A fine grid near the centerline is important since it is expected that significant velocity and temperature gradients exist there.

Note that the grid size has been chosen after a careful examination of the grid dependency of the solution. This examination has been performed by making the grid more and more fine for exactly the same hydrodynamic problem, until grid refinement seized to yield noticeable changes in the flow field, including quantitative parameters like the frequency of vortex shedding in the wake of the plate. The finest grid tried had as much as $90 \times 120 \times 22 \times 2 = 237,600 \times 2$ elements for a $5H$ high chimney alone, and the smallest elements near the plate were as small as 0.2 mm. This grid provided essentially the same results as that finally chosen, but needed much longer calculation times.

The calculations were performed with a heat-transfer coefficient of 1.0 W/m^2 K through the walls, determined experimentally. Additional calculations for the adiabatic wall showed essentially the same temperature field; however, the air adjacent to the walls became slightly warmer.

We have already noted that the experiments performed in the present study, including both measurements and visualization, show considerable fluctuations of the velocity and temperature inside the system. In order to take into account these fluctuations, an unsteady form of the governing equations has been solved [13]. The numerical approach included second-order upwind schemes for the momentum and energy equations, chosen to provide greater accuracy. In addition, second-order discretization is important where the flow crosses the grid lines obliquely, in order to reduce numerical diffusion. Since natural convection with relatively high Rayleigh numbers (Ra about 10^9) is encountered, a second-order pressure interpolation scheme has been used. The SIMPLE algorithm has been used for pressure–velocity coupling.

General validity of the numerical approach has been verified solving the model hydrodynamic problem of vortex shedding from a plate ("von Karman vortex street") at various plate thickness, length-to-thickness ratio, and flow velocity, expressed through the plate-thickness-based Reynolds number and dimensionless shedding frequency. Additional model problem was that of shedding suppression by heating of the plate. These model problems were chosen because independent experimental and numerical results had been reported on them in the literature, including the recent works by Eisenlohr and Eckelmann [14] and Hourigan et al. [15] on vortex shedding from long plates, and Noto et al. [16], Schumm et al. [17] and Lecordier et al. [18] on the thermal effects in vortex shedding. An additional reason for the choice of these model problems was the fact that the flow in the chimney is an induced one, thus bearing features of both free and forced convection.

The model problems are introduced and discussed in Appendix A, and shown in Figs. 10–13. There, it is shown that, in general, the results obtained by the present method are quite similar to those reported in the literature. Therefore, the present numerical approach may be considered quite reliable.

Examples of the numerical results are presented in Figs. 2d, 3 and 7c for the temperatures, and in Figs. 4a–7b for the velocities.

4. Results and discussion

4.1. Temperature distribution

For the lowest configuration, $2H$, the temperatures were measured across the chimney (normal to the plate) at the heights 1^+H and $2H$ by the thermocouples denoted $TC1^+$ and TC2. For the second configuration, $3H$, the thermocouples $TC1^+$, TC2, and TC3 were used. The thermocouples $TC1^+$, TC2, TC3, TC4, and TC5 have been used for $5H$ and for $9H$.

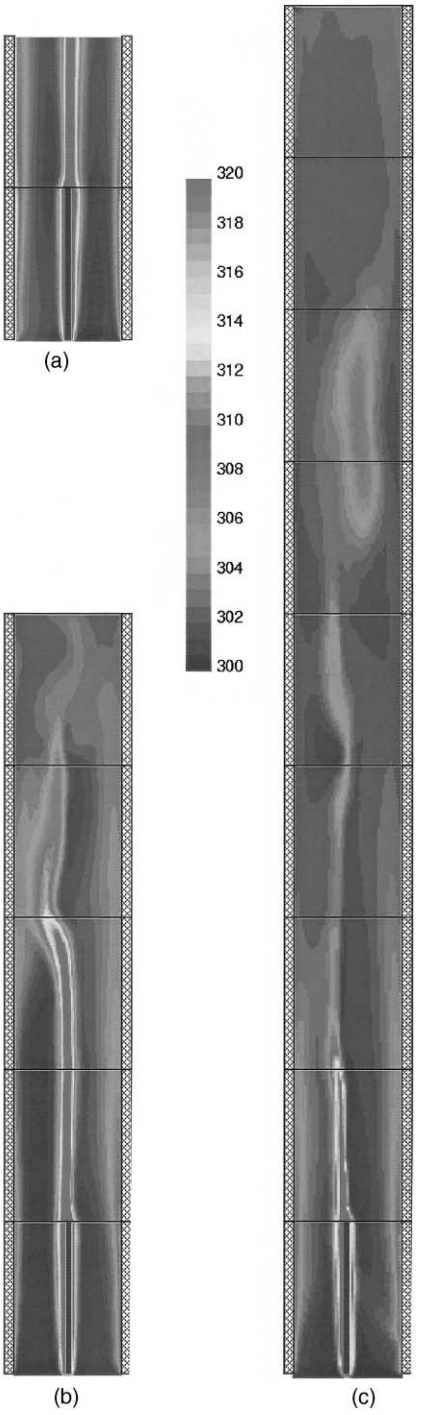

Fig. 3. Simulated instantaneous temperature distributions for different chimney heights: (a) $2H$, (b) $5H$ and (c) $9H$.

Fig. 2a–c shows the examples of air mean temperature profiles, measured at various levels inside the chimney for the heat input of 40.5 W, and chimney

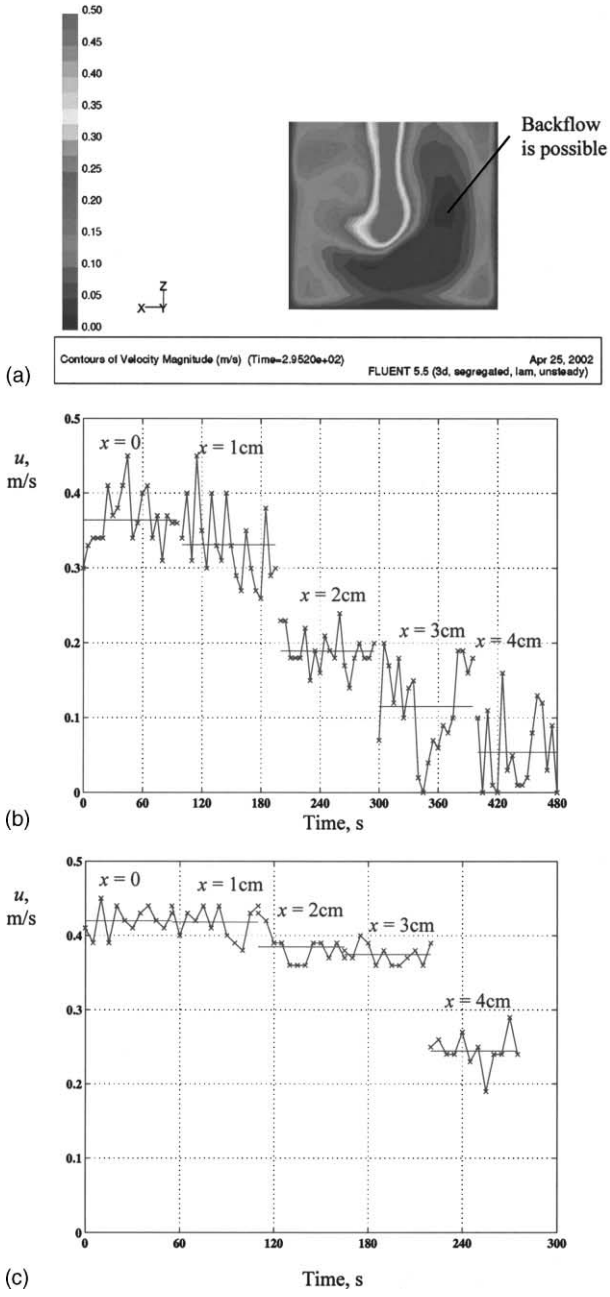

Fig. 4. Examples of velocity distribution: (a) simulated velocity distribution at a horizontal plane—exit of the chimney $2H$ high (half the system is shown as simulated), (b) velocity fluctuations and local mean velocities of air measured across the chimney at the exit of the $2H$ high chimney and (c) velocity fluctuations and local mean velocities of air measured across the chimney at the height of $5H$ in the $9H$ high chimney.

heights of $3H$, $5H$, and $9H$, respectively. In order to eliminate the effect of the ambient, the indicated temperatures relate to the measured difference between inside and outside.

One can see from Fig. 2 that the temperature of air at any point above the plate decreases considerably as the height of the chimney increases. This trend is observed for all the thermocouples placed at the centerline of the chimney. The decrease in the air temperature means, for the constant heat output from the plate, that the air flow rate increases significantly with the height of the chimney. This increase causes considerable decrease in the

temperature of the plate—the measured temperatures of the plate for the $2H$ and $9H$ chimneys differ as much as about 10 °C.

Fig. 2 also shows evolution of the air temperature profiles across the chimney. Just above the plate, there is a sharp peak in the temperature profile at the centerline, within the hot air which is shed from the plate. Farther from the centerline, the temperature drops steeply and remains at almost the same level. Near the walls, opposite to the plate, the temperature increases slightly. This increase is caused by convection at the walls which are heated by direct radiation from the plate. As the air flows upwards, the temperature profile gradually changes. The peak becomes less and less sharp, and the temperature gradients in the cross-sections become smaller. Above the plate the effect of radiation is insignificant. Therefore, in a chimney that is high enough a smoother monotonic mean temperature profile is established.

The mean temperature profiles obtained at different power outputs from the plate demonstrate shapes similar to those at 40.5 W, but differ quantitatively, as expected.

Fig. 3 shows the simulated instantaneous temperature distributions for the chimney heights of $2H$, $5H$, and $9H$. One can see that these instantaneous distributions follow, in general, the same trends as the measured mean temperatures. In particular, it is true for the temperature values along the centerline of the chimney, the shape of the temperature profiles at different heights, and the effect of radiation.

One can also see from Fig. 3 that, unlike the mean profiles, the instantaneous temperature distributions are not symmetrical. This result is due to the oscillating character of the flow, as is discussed in the following. This character expresses itself also in Fig. 2d, where the simulated mass-averaged temperature of the air leaving a $9H$-high chimney is shown. A very good agreement is observed between this temperature and the mean temperature represented by TC5 in Fig. 2c for the same chimney. Note that the latter is just a mean of the measured values; since the velocity at the centerline is higher than near the walls, the experimental mass-average value should have been even closer to the simulated one.

4.2. Velocity field

Considering the temperature distributions discussed above, one can conclude that they are caused by the velocity field. Analysis of the velocity measurements and simulations, accompanied by the visualization, shows that this is, indeed, the case.

Fig. 4a shows the simulated velocity distribution at a horizontal plane—exit of the chimney $2H$ high (half the system is shown as simulated). The velocity has a pronounced maximum over the plate, which corresponds both to the simulated temperature distribution of Fig. 3a and the measured temperature profiles at this chimney height. Farther from the plane of the plate, the velocity becomes much lower, but it can rise again closer to the walls that are heated by radiation.

The velocities measured at the same location, i.e. the open top cross-section of the $2H$ high chimney, show very similar behavior, as demonstrated in Fig. 4b. The measurements were performed at five points of distance x, normal to the plane of the plate. At each point, the velocity readings were taken for approximately 50–70 s. One can see steep decrease in the mean velocity. For a higher $9H$ chimney, Fig. 4c, the velocity profile develops downstream and becomes flatter, likewise the temperature profile discussed above.

Fig. 4b–c presents also the fluctuating velocity, but these measurements cannot yield the real period of oscillations because of the relatively low sampling frequency. However, they provide some indication of the very strong local oscillations in the flow velocity. Additional feature that can be detected from Fig. 4b is the zero flow velocity possible at $x = 3$–4 cm. Since the anemometer shows the absolute value of the velocity, this result means that backflow can exist at this location. The numerical simulation shows that, indeed, backflow occurs from time to time at that location as indicated in Fig. 4a. It is similar to the episodic and time-dependent cold inflow detected and discussed by Fischer and Torrance [5].

As mentioned above, velocity measurement cannot give a full picture of the velocity fluctuations. In this problem, smoke visualization proves to be of great help. Fig. 5a shows a typical smoke pattern at the entrance of the symmetrical enclosure, where the smoke is introduced at point S1, as denoted in Fig. 1. As visualized in Fig. 5a, one can see that the smoke flows mostly along the bottom and then turns upwards, to the chimney. A small part of smoke is entrained into the clockwise rotating vortex, located at the upper right corner of Fig. 5a, around point S4 as denoted in Fig. 1. Fig. 5b, which shows a simulated instantaneous flow field inside the enclosure, supports this result. In addition, Fig. 5b shows that in spite of the geometrical symmetry, the flow field inside the enclosure is typically asymmetric.

This point is further illustrated in Fig. 6, which shows the smoke visualization just above the tip of the heating plate, with smoke introduction into the chimney at a point beneath the plate, denoted by S2 in Fig. 1. The flow of smoke was observed through the transparent window of the chimney. The plate tip appears at the bottom of the frames shown in the upper row of Fig. 6. The light was provided by two optic fibers, through two small drills located symmetrically in the side walls of the chimney. Actually, these were the drills used for thermocouple $TC1^{+}$ in the temperature

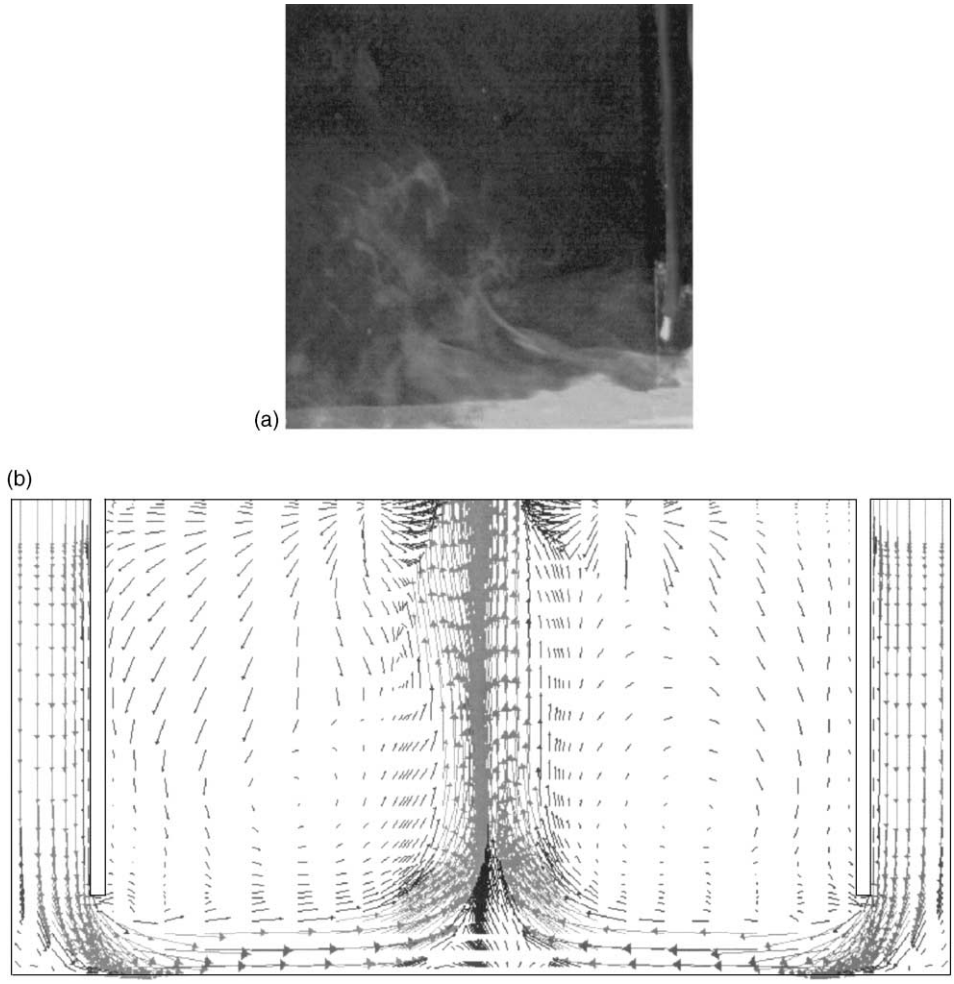

Fig. 5. Flow inside the enclosure: (a) typical smoke pattern at the entrance of the symmetrical enclosure, where the smoke is introduced at point S1 and (b) simulated instantaneous flow field inside the enclosure.

measurements. The recording rate was 125 frames/s. The time interval between frames 1 and 3 is 0.44 s. One can see that although the smoke entered the system symmetrically relative to the plate, its flow is not uniform. As visualized in Fig. 6, in frame 1 smoke flows mostly to the left of the plate, in frame 3 the smoke flows to the right of the plate, and in frame 2 the smoke flow is quite symmetrical. This result can be explained considering the corresponding simulated flow field also shown in Fig. 6. One can see from the velocity field that at the leading edge of the plate, where the smoke is let into the system, the velocity can be considerably higher to the right of the plate, to the left of it, or about the same from both sides. As a result, the smoke is entrained mostly to the left, to the right, or equally to the both sides. Thus, Figs. 5 and 6 show that the flow in the box and in the vicinity of the plate has a fluctuating character and is generally not symmetrical.

Consider now the wake of the plate. It is shown in Appendix A that the wake flow can be characterized by alternating vortices which are suppressed when the plate is heated, leading to a stable wake. Fig. 7 reveals that in our case the wake is neither a vortex street, nor a stable pattern aligned with the flow direction.

Fig. 7a presents the result of image processing of two frames taken during flow visualization when smoke filled the whole enclosure. The smoke in the illuminated region is represented by white fields, while the wake is black. The tip of the plate is shown, as well. One can see a triangle-shaped pattern above the plate, followed by a thin "tail", which shifts from left to right. This feature is easily seen also in the simulation of the flow above the plate, shown in Fig. 7b. It appears that the triangle pattern is formed by two counter-rotating vortices, which do not detach but rather shift, while the tail is formed by the main flow. The temperature distribution

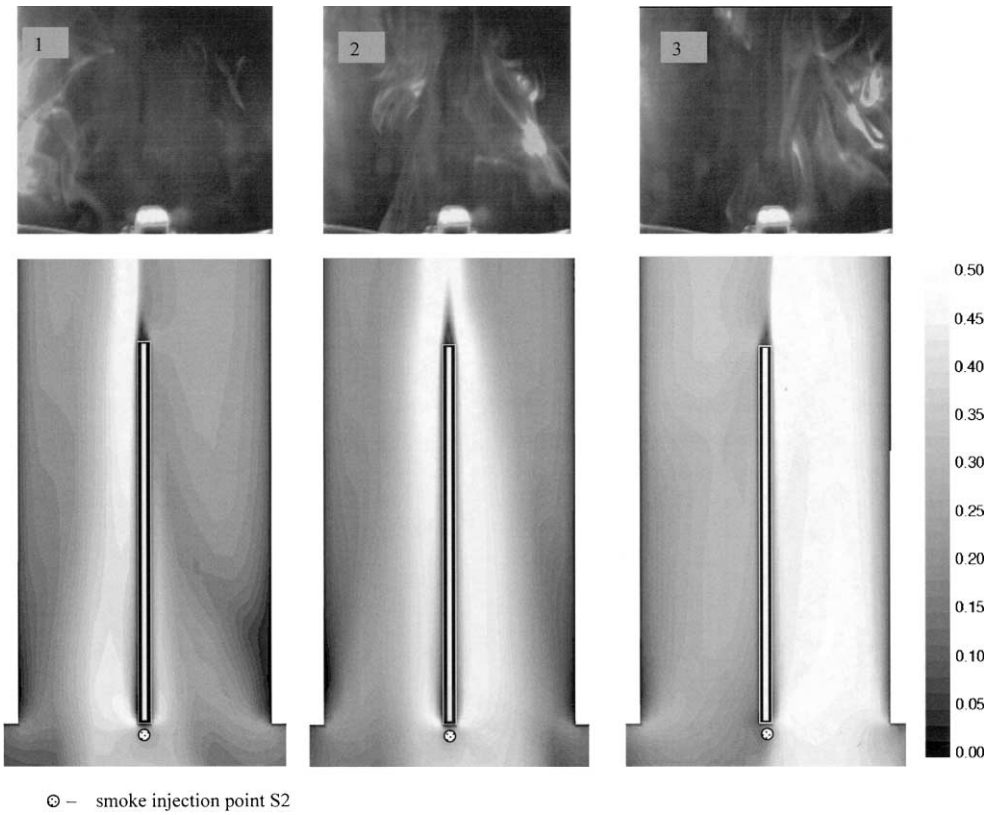

Fig. 6. Smoke visualization just above the tip of the heating plate, with smoke introduction at point S2 (upper row) and numerical simulation of the flow field (lower row).

shown in Fig. 7c corresponds to this flow pattern, showing that the wake is the region of highest temperature (shown by the darkest region) which also shifts.

The patterns above the plate are a further indication of the pulsating character of the flow inside the chimney. This character, however, is not similar to the von Karman shedding. In our opinion, it is quite possible that the instability of the flow in our case is related to the fact that the system has two ports, and the flow inside it is determined by two streams coming from the opposite directions. This point needs further analysis.

4.3. Plate temperature and air flow rate

Fig. 8 shows the measured time-average temperature of the heated plate at $2H$, $3H$, $4H$, $5H$, and $9H$, versus the numerical predictions for $2H$, $5H$, and $9H$. Since the emissivity of the plate was not measured directly, we present the temperature of the plate in a normalized form, where the normalized temperature is defined as $(T_p - T_{in})/(T_{p,2H} - T_{in})$, i.e. it equals unity for the plate in the $2H$-high chimney (the lowest considered), and the absolute values of $T_{p,2H}$ are not necessarily identical in the measurement and simulation. Comparison of the trend lines drawn in Fig. 8 for the measured and simulated values show a very good agreement between the two.

Finally, Fig. 9 shows the mass flow rate of air, predicted by the numerical simulation, and the flow rate estimated from the experiments vs. the chimney height in H units. The point of $H = 0$ is the theoretical result for an identical plate in an infinite reservoir, corresponding to a mass flow rate of about 0.63 g/s. Since the mass flow rate was not constant in time but had a fluctuating character, the two curves show the highest and lowest values, respectively, of the simulated overall mass flow rate for each chimney height. The experimental mass flow rate, indicated by solid triangles, was roughly estimated by using the measured velocity profiles for $5H$ and $9H$. As these profiles were measured only at the two orthogonal symmetry planes of the chimney, interpolation was used. Unfortunately, it was not possible to do the same for small chimney heights, because of the steep velocity profiles there. For the two points, the deviation between the experimental estimation and the mean simulated value is less than 20%, which is an adequate

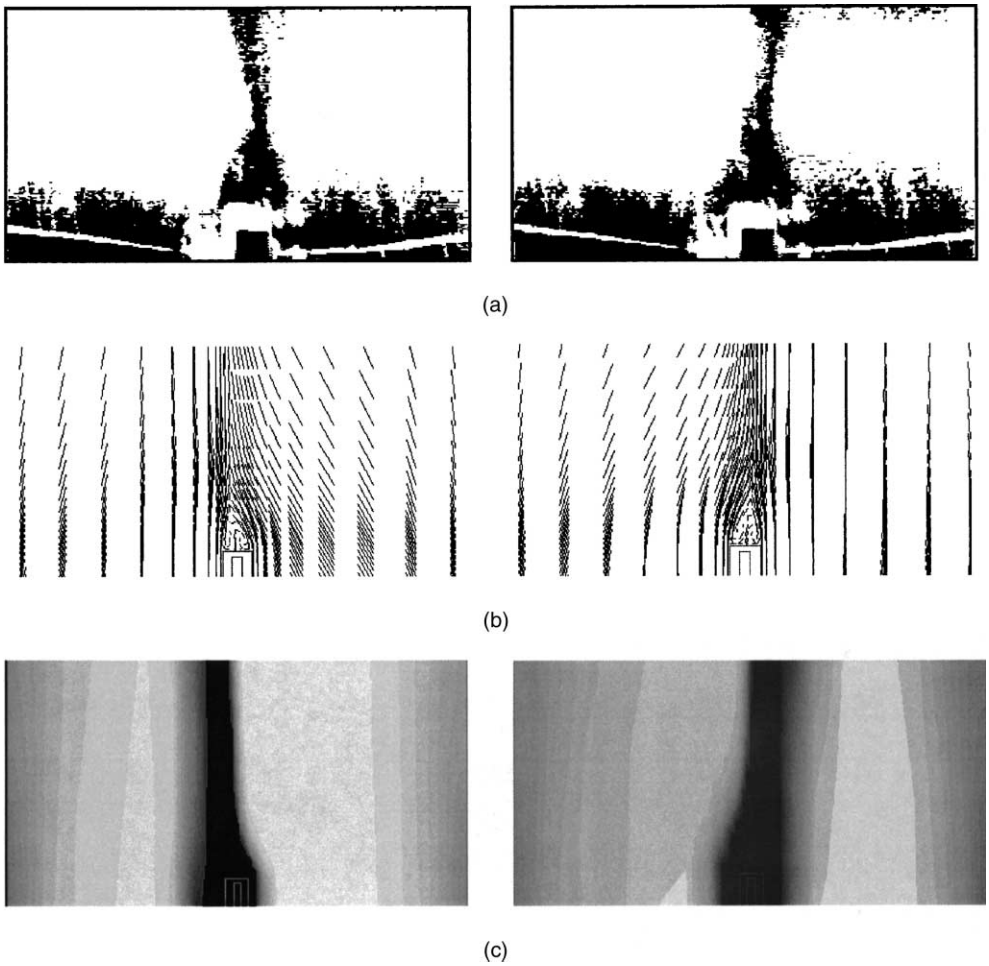

Fig. 7. Instantaneous flow fields in the wake of the heated plate: (a) image-processed flow visualization, (b) simulated velocity field and (c) simulated temperature distribution.

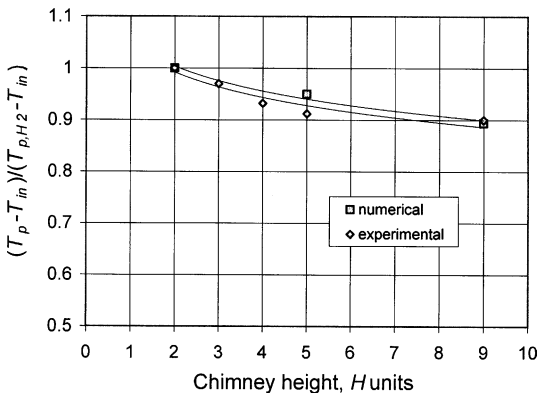

Fig. 8. Measured and numerically calculated values of the heated plate temperature, as a function of chimney height in H units.

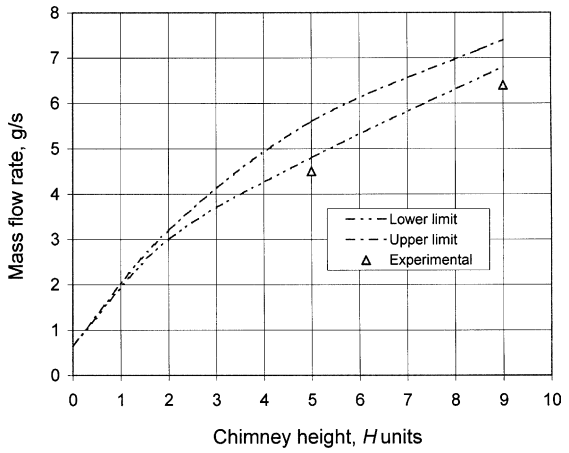

Fig. 9. Air mass flow rate in the chimney, estimated experimentally and calculated numerically, as a function of chimney height. The two curves show the upper and lower limits of the fluctuating flow rate.

agreement for engineering purposes. This means that the pumping effect of the heated plate in the chimney can be predicted by simulation for various system configurations and chimney heights.

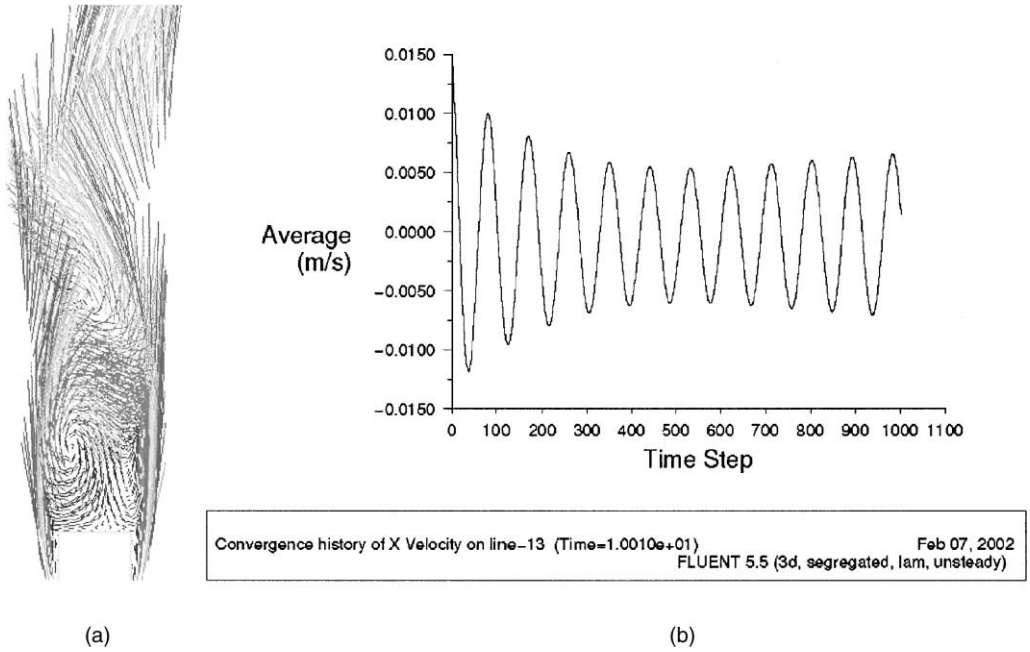

Fig. 10. Sustained vortex shedding from a cold body of square cross-section: (a) instantaneous velocity field and (b) regular oscillations of the air velocity normal to the plate.

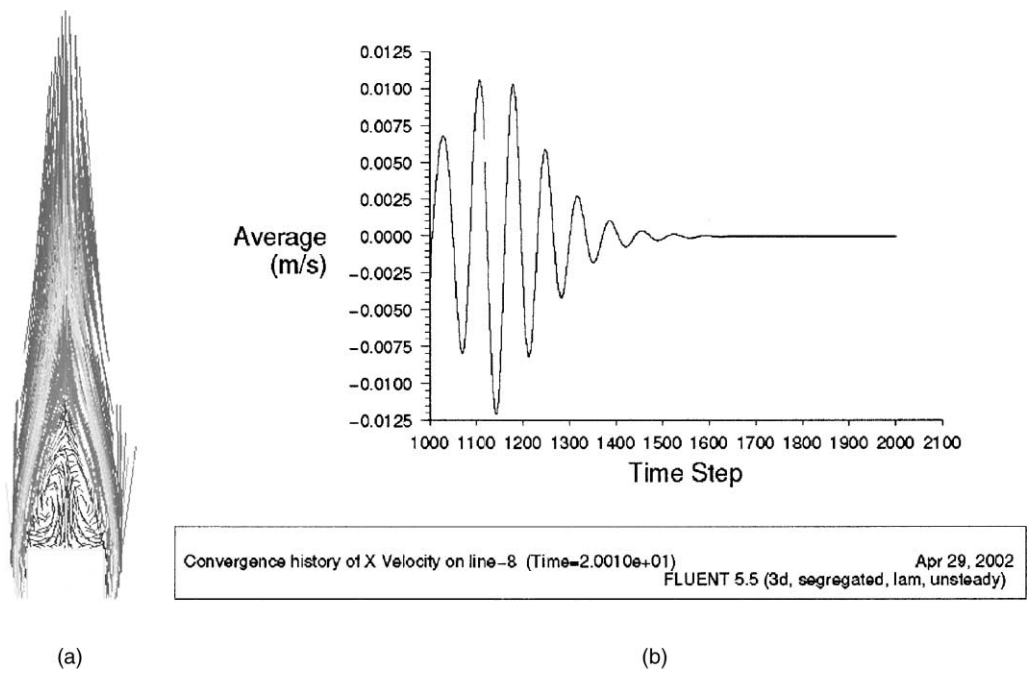

Fig. 11. Stable vortex pattern above a heated body of square cross-section: (a) velocity field and (b) oscillations fading as a result of heating.

The variation of flow rates with chimney height demonstrates the practical essence of the work presented herein: a chimney enhances the flow rate, from about 0.63 g/s on a plate in an infinite reservoir, to about 6–7 g/s in a 1350 mm high chimney in a system of that size and configuration.

5. Closure

Natural convection from a vertical electrically heated plate, placed in a chimney, has been investigated both experimentally and numerically. Effect of chimney height on heat transfer rates from the plate, and on the temperature and flow field inside the chimney has been studied in detail. Local mean and fluctuating temperatures and velocities have been experimentally obtained for various locations inside the chimney, providing, along with the flow visualization, a comprehensive picture of the phenomena.

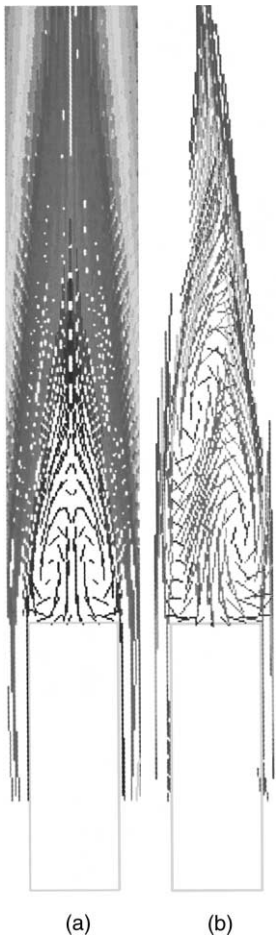

Fig. 12. Flow in the wake of a heated short thin plate: (a) stable pattern and (b) vortex shedding.

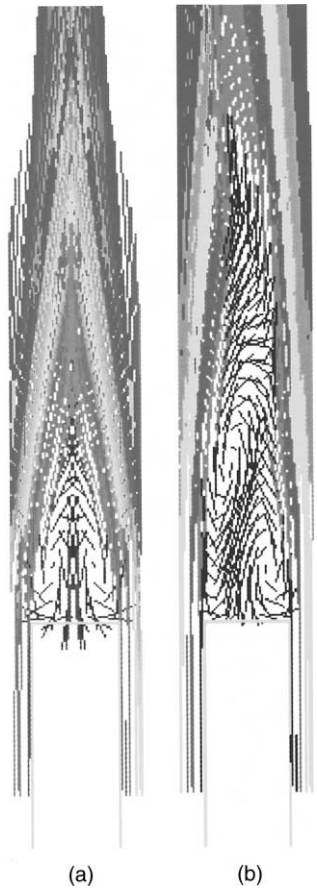

Fig. 13. Flow in the wake of a heated long thin plate: (a) stable pattern and (b) vortex shedding.

The computer simulations of the flow and temperature fields were performed and compared with the experimental results. The overall mass flow rate through the chimney, which reflects the pumping power of the heated plate, was similar in the experiments and the numerical simulations, and increased with the height of the chimney. For the particular size and configuration of the system employed herein an enhancement of the air flow rate up to 10 times was achieved.

Appendix A

The model problem used for the verification of the numerical method was that of vortex shedding behind a bluff body.

The approach adopted herein was to solve the hydrodynamic problem for the body identical to the plate used in this study, in the geometry identical to that of the experimental set-up. However, for the comparison with

the findings from the literature, it was important to involve other shapes of the body. Thus, the following three cross-section shapes have been used: a square cylinder 15×15 mm, a plate 5×15 mm, and a plate 5×150 mm, which is identical to the plate in the main study. The velocities of the flow were chosen to be similar to those encountered in the main study. Three-dimensional transient simulations were performed.

Fig. 10a shows the velocity field above the square cylinder placed in the chimney with the mean air velocity of 0.1 m/s. The Reynolds number based on the body thickness, Δ, is equal to 100. One can see that a von Karman vortex street develops behind the body. Fig. 10b shows a quite regular oscillating pattern represented by the velocity in the x-direction (normal to the flow in the plane of Fig. 10a) at a point on the centerline above the body. The period of oscillations is 0.9 s.

The situation changes drastically when the plate is "instantly" heated to 10 °C above the ambient. The vortex shedding stops, and two steady vortices are formed on the top of the body, as shown in Fig. 11a. This result is in full agreement with the experimental findings of Noto et al. [16] and Lecordier et al. [18] on the effect of the body temperature on its wake. The x-velocity at the same point decays to zero, as shown in Fig. 11b. Note that the time intervals in Figs. 10b and 11b are 10 s each, and Fig. 11b follows Fig. 10b.

Fig. 12 represents the results for a plate 5×15 mm at ambient temperature. When the same velocity of 0.1 m/s is used, there is no shedding, because the Reynolds number decreases to 30. For the same Reynolds number of 100, the velocity should now be 0.3 m/s, as in Fig. 12b. Here, the vortex street is observed once again. However, the period of oscillations is now 0.12 s. Thus, at the same thickness-based Reynolds number, two bodies with the thickness ratio of 3:1 have the frequency shedding ratio of $0.9/0.12 = 7.5$, which is in good agreement with the correlation of Eisenlohr and Eckelmann [14] and analysis of Hourigan et al. [15].

Fig. 13a shows that for the plate of 5×150 mm at the same velocity of 0.3 cm/s and thickness-based Reynolds number of 100, stable vortices are observed. The velocity should be increased to 0.5 m/s ($Re = 170$) in order to obtain a von Karman pattern. This result is, once again, in agreement with the analysis of Eisenlohr and Eckelmann [14]. There, it is shown that the characteristic length used both in the Reynolds number and the dimensionless frequency (or the Strouhal number) should be based on a sum of the plate thickness and the displacement thickness of the boundary layer along the plate, rather than on the plate thickness alone. Since the displacement thickness is obviously larger for a longer plate, while the plate itself is relatively thin, there is the above-mentioned difference in the results of Figs. 12 and 13.

The examples discussed in this Appendix show that the numerical method used in the present study is quite reliable in the prediction of complex flow patterns encountered in flows around bluff bodies. One can also conclude that it is quite improbable that a von-Karman-type shedding takes place in the induced convection discussed in the main text, since the mean velocities there are typically below 50 cm/s while the temperature of the plate is typically about 100 °C above the ambient.

References

[1] V. Dubovsky, G. Ziskind, S. Druckman, E. Moshka, Y. Weiss, R. Letan, Natural convection inside ventilated enclosure heated by downward-facing plate: experiments and numerical simulations, International Journal of Heat and Mass Transfer 44 (2001) 3155–3168.

[2] G. Ziskind, V. Dubovsky, R. Letan, Ventilation by natural convection of a one-story building, Energy and Building 34 (2002) 93–104.

[3] R. Letan, V. Dubovsky, G. Ziskind, Passive ventilation and heating by natural convection in a multi-story building, Building and Environment 38 (2003) 197–208.

[4] G. Ziskind, V. Dubovsky, R. Letan, Removal of contaminants from underground spaces by induced ventilation, ASCE Journal of Environmental Engineering 128 (2002) 673–688.

[5] T.S. Fisher, K.E. Torrance, Experiments on chimney-enhanced free convection, ASME Journal of Heat Transfer 121 (1999) 603–609.

[6] T.S. Fisher, K.E. Torrance, K.K. Sikka, Analysis and optimization of a natural draft heat sink system, IEEE Transactions on Components, Packaging and Manufacturing Technology—Part A 20 (1997) 111–119.

[7] T.S. Fisher, K.E. Torrance, Free convection limits for pin-fin cooling, ASME Journal of Heat Transfer 120 (1998) 633–640.

[8] E.M. Sparrow, S. Shah, C. Prakash, Natural convection in a vertical channel: I. Interacting convection and radiation. II. The vertical plate with and without shrouding, Numerical Heat Transfer 3 (1980) 297–314.

[9] S.E. Haaland, E.M. Sparrow, Solutions for the channel plume and the parallel-walled chimney, Numerical Heat Transfer 6 (1983) 155–172.

[10] A.G. Straatman, J.D. Tarasuk, J.M. Floryan, Heat transfer enhancement from a vertical, isothermal channel generated by the chimney effect, ASME Journal of Heat Transfer 115 (1993) 395–402.

[11] G.A. Shahin, J.M. Floryan, Heat transfer enhancement generated by the chimney effect in systems of vertical channels, ASME Journal of Heat Transfer 121 (1999) 230–232.

[12] Y. Glat, A. Aviv, Ventilation of an enclosure by natural convection with hot vertical plate in the chimney, Graduation project 00-04, supervised by R. Letan, Y. Weiss, Heat Transfer Laboratory, Department of Mechanical Engineering, Ben-Gurion University of the Negev, 2000.

[13] FLUENT User's Guide, Version 5.5, Fluent Incorporated.

[14] H. Eisenlohr, H. Eckelmann, Observations in the laminar wake of a thin flat plate with a blunt trailing edge, in: R.K. Shah, E.N. Ganić, K.T. Yang (Eds.), Experimental Heat Transfer, Fluid Mechanics, and Thermodynamics, Elsevier Science Publishing Co., New York, 1988, pp. 264–268.
[15] K. Hourigan, M.C. Thompson, B.T. Tan, Self-sustained oscillations in flows around long blunt plates, Journal of Fluids and Structures 15 (2001) 387–398.
[16] K. Noto, H. Ishida, R. Matsumoto, A breakdown of the Karman vortex street due to the natural convection, in: W.J. Yang (Ed.), Flow Visualization III, Hemisphere, Washington DC, 1985, pp. 348–352.
[17] M. Schumm, E. Berger, P.A. Monkewitz, Self-excited oscillations in the wake of two-dimensional bluff bodies and their control, Journal of Fluid Mechanics 271 (1994) 17–53.
[18] J.-C. Lecordier, L.W.B. Browne, S. Le Masson, F. Dumouchel, P. Paranthoën, Control of vortex shedding by thermal effect at low Reynolds numbers, Experimental Thermal and Fluid Science 21 (2000) 227–237.